

Facile synthesis and gas sensing performances based on nickel oxide nanoparticles/multi-wall carbon nanotube composite

Nan Chen¹ · Qing Li¹ · Yuxiu Li¹ · Dongyang Deng¹ · Xuechun Xiao^{1,2} · Yude Wang^{1,2}

Received: 22 May 2015 / Accepted: 11 July 2015 / Published online: 16 July 2015
© Springer Science+Business Media New York 2015

Abstract A facile method was applied to prepare NiO nanoparticles/multi-walled carbon nanotubes (MWCNTs) nanocomposite. The structure and morphology of the as-prepared nanocomposite were characterized by X-ray diffraction, Raman spectrum, scanning electron microscopy, transmission electron microscopy (TEM) and high-resolution TEM. It was indicated that NiO nanoparticles with size of 10–30 nm were tightly decorated on the MWCNTs. A chemoresistive gas sensor using NiO nanoparticles/MWCNTs nanocomposite as sensitive material was fabricated on an alumina tube with Au electrodes and platinum wires. The gas-sensing properties of NiO nanoparticles/MWCNTs nanocomposite were evaluated for volatile organic compound vapors (VOCs). The electrical resistance is found to be dramatically decreased by three orders of magnitude compared to a sensor based on NiO nanoparticles free MWCNTs. The highest response values of the nanocomposite were obtained at operating temperature of 180 °C. NiO/MWCNTs sensor shows much better performance compared to the NiO sensor and the VOCs responses are found to be several times higher than that of a NiO nanoparticles sensor.

1 Introduction

As an important p-type semiconductor, NiO has attracted considerably investigation because of its unique properties such as a wide band-gap (3.6–4.0 eV), an measurable electrical conductivity change accompanied with chemical reactions on the surface of materials, which makes it a potential application to gas sensors, with many related articles published [1]. Nevertheless, the diverse structures of NiO (nanoparticles, nanosheets, nanotubes, fibers, hollow spheres, nanowires, etc.) [2–6], appropriate doped-NiO (Pt, Au, Fe, and Zn) [7–9], and NiO composited with other oxide semiconductors (ZnO, SnO₂, and PdO) [10–12] have been developed in recent years as sensitive materials for ethanol, acetone, methanol, formaldehyde, CO and NH₃. The metal-oxide-based gas sensors need to be operated at relatively high temperatures. Nickel oxide has been used for many years in sensing application with operating temperature around 300–350 °C. The high operating temperatures may cause coalescence and structural changes which leads to sensor instability and response variation. To overcome the disadvantages of NiO-based gas sensors, the research on preparation, doping, and composing of other metal oxides had been done. However, there are many challenges and issues that arise and stand around materials under development from the viewpoint of their synthesis and performances.

Carbon nanotubes (CNTs) having unique geometry and amazing structural features appear as a potential candidate for gas sensors. The big advantage of CNT-based gas sensors, when compared to conventional metal oxide chemical sensors, is that they can operate at low operating temperature [13]. Nevertheless, a major weakness of CNT-based gas sensors is slow recovery from the CNT and analyte interaction, needing several hours to release the adsorbed analyte at low operating temperature before they are reused. CNTs

✉ Yude Wang
ydwang@ynu.edu.cn

¹ School of Physical Science and Technology, Yunnan University, Kunming 650091, People's Republic of China

² Yunnan Province Key Lab of Micro-Nano Materials and Technology, Yunnan University, Kunming 650091, People's Republic of China

composted with metal oxides can exhibit the different physical properties than those of neat CNTs. The sensing properties of CNT-based sensors can be improved by functionalization in form of surface modifications of the CNTs by appropriate metals or metal oxides [14]. In the last few years, hex-WO₃/MWCNTs [15], TiO₂/MWCNTs [16], SnO₂/MWCNTs [17, 18], ZnO/MWCNTs [19], and NiO/MWCNTs [20] have been using as gas sensing materials for gas sensors and exhibited good gas sensing properties, such as high sensitivity, capability of gas adsorption, and low operating temperature. Jung et al. [20] reported that the MWCNT/NiO composite acting as gas sensor showed a higher sensitivity at room temperature for H₂ gas. However, to our best knowledge, so far there is no report on the detection of VOCs gas over NiO/MWCNTs composites. In the present work, thus, considerable efforts are dedicated toward the enhancement of the low-operating-temperature VOCs gas response of NiO/MWCNTs composites synthesized by a simple fabrication method. The high-quality MWCNTs forming a composite with the nickel oxide shows good VOCs sensing characteristics.

2 Experimental

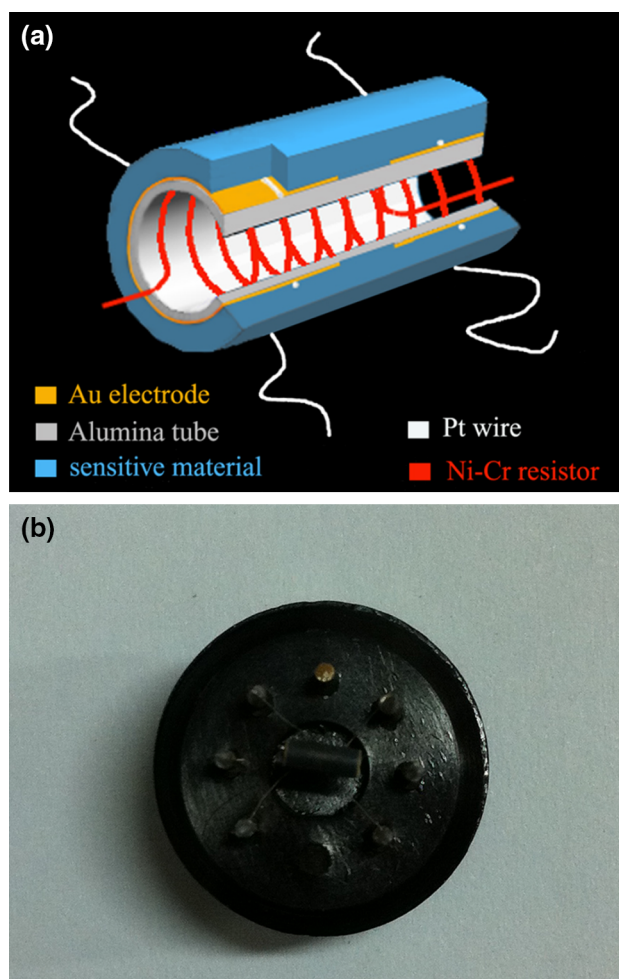
All the chemical reagents used in the experiments were obtained from commercial sources as guaranteed-grade reagents and used without further purification.

The NiO/MWCNTs nanocomposite was prepared by a simple chemical precipitation followed by thermal annealing. The synthetic procedure was as follows: (1) the refluxed MWCNTs treated in 68 wt% HNO₃ for 24 h were suspended in 25 ml deionized water by ultrasonication for 2 h; (2) 10 ml NH₃·H₂O (25 wt% solution) was mixed with the distilled deionized water; (3) ammonium hydroxide was then dropped into the MWCNTs suspension with stirring for 4 h; (4) the synthesis mixture was then added into the 0.2 M 25 ml Ni²⁺ solution of NiCl₂ diluted with distilled deionized water, producing a suspension; (5) after stirring 2 h, the obtained precipitant was further centrifuged to separate the nanocomposite of nickel hydroxide and MWCNTs. After dried in air, these samples were annealed at 400 °C for 2 h in air. The molar ratio of Ni²⁺:MWCNTs was 1.0:1.0.

X-ray diffraction (XRD) patterns were obtained on a Rigaku D/MAX-3B powder diffractometer with copper target and K_α radiation ($\lambda = 1.54056 \text{ \AA}$). The samples were scanned from 10° to 90° (2 θ). Scanning electron microscopy (SEM) characterization was performed with FEI QUANTA200 microscope operating at 15 kV. The Raman spectra was recorded with a Renishaw inVia Raman microscope, equipped with a CCD (charge coupled device) with the detector cooled to about 153 K using liquid N₂. The laser power was set at 30 mW and the

spectral resolution was 1 cm⁻¹. The samples for SEM were prepared by dispersing the final powders in the conductive glue; this dispersing was then sprayed with carbon. Transmission electron microscopy (TEM) measurement was performed on a Zeiss EM 912 Ω instrument at an acceleration voltage of 120 kV. The samples for TEM were prepared by dispersing the final samples in distilled deionized water; this dispersing was then dropped on carbon-copper grids covered by an amorphous carbon film. To prevent agglomeration of nanostructures, the copper grid was placed on a filter paper at the bottom of a Petri dish.

In order to prepare series of sensors, we elected the indirect-heating structure shown in Scheme 1 [21, 22]. As-prepared NiO nanoparticles/MWCNTs nanocomposite and NiO nanoparticles used as sensitive layer with a thickness of about 0.6–0.8 mm were deposited on an alumina tube (4 mm in length and 1.2 mm in diameter) with Au electrodes and platinum wires, respectively. The thickness of the sensitive body, which was dried and sintered in air at



Scheme 1 a Sketch of the structure of a typical NiO nanoparticles/MWCNTs nanocomposite gas sensor; b photograph of the gas sensor

400 °C for 2 h in N_2 , was about 0.5 mm. A Ni–Cr alloy crossed alumina tube was used as a heating resistor (R_H). This resistor ensured both substrate heating and temperature control with the different heating voltage (V_H). Before measuring the gas sensing properties, the gas sensors were aged at 150 °C of operating temperature for 150 h in dry air. The electrical response of the sensor was measured with an automatic test system, controlled by a personal computer. The export signal of the sensor was measured by using a conventional circuit (Scheme 2) in which the element was connected with an external resistor in series at a circuit voltage of 5 V. According to Scheme 2, the electrical resistance of sensor can be obtained as following:

$$R = \frac{5 - V_o}{V_o} \cdot R_L$$

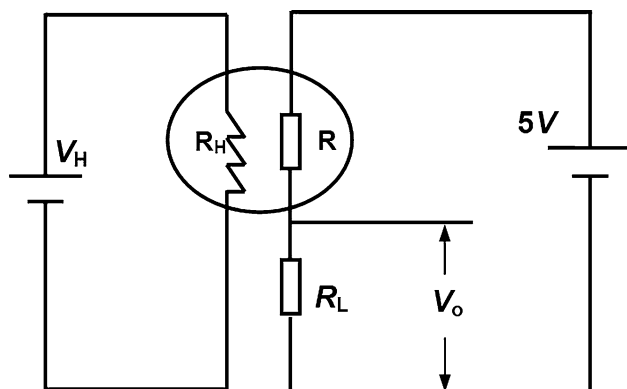
where R is the resistance of the sensor, R_L is a constant load resistance unchanged with the surrounding gas partial pressure, V_o is the sensor export voltage. The gas response β was defined as the ratio of the electrical resistance in gases (R_g) to that in air (R_o):

$$R_o = \frac{5 - (V_o)_{air}}{(V_o)_{air}} \cdot R_L, \quad R_g = \frac{5 - (V_o)_{gas}}{(V_o)_{gas}} \cdot R_L, \quad \beta = \frac{R_g}{R_o}$$

where $(V_o)_{air}$ is the export voltage in air, and $(V_o)_{gas}$ is in VOCs, such as isopropanol, acetone, ethanol, formaldehyde, and methanol. As a comparison, NiO nanoparticles obtained from commercial source were used as sensing material to fabricate gas sensor and investigated the performance to VOCs gases.

3 Results and discussion

The phase purities of the products were examined by X-ray diffraction (XRD) measurement performed on Rigaku X-ray diffractometer with Cu $K\alpha$ radiation. The XRD patterns



Scheme 2 Schematic diagram of testing principle for NiO nanoparticles/MWCNTs nanocomposite gas sensor. V_H is heating voltage and R_H is heating resistance

of the $Ni(OH)_2$ /MWCNTs and NiO /MWCNTs show the diffraction peaks in Fig. 1. It can be perfectly indexed to a hexagonal phase (space group: $P\bar{3}m1$ (164)) of β - $Ni(OH)_2$ with lattice constants $a = 3.126 \text{ \AA}$, $c = 4.605 \text{ \AA}$ (JCPDS No. 14-0117) and a cubic phase (space group: $Fm\bar{3}m$ (225)) of NiO with lattice constants $a = 4.177 \text{ \AA}$ (JCPDS No. 47-1049), respectively. On the other hand, it can be clearly seen a diffraction peak at about 26° (2θ) before and after the annealing treatment, which attributed to the (002) reflection of highly structured graphitic carbon of the CNTs [20]. Compared with $Ni(OH)_2$ /MWCNTs and NiO /MWCNTs, XRD pattern of the heat-treating sample at 400 °C for 2 h in air shows new peaks, which can be matched well with NiO . It shows that mix-phase $Ni(OH)_2$ and NiO can be obtained by calcination of as-synthesized $Ni(OH)_2$ at 400 °C for 2 h. All diffraction peaks of XRD pattern can be indexed to phases of NiO and CNTs, respectively, indicating that the $Ni(OH)_2$ had been converted into the cubic NiO phase completely during the calcination conversion process. The annealing treatment had no significant influence on the graphite structure of the CNTs.

The Raman spectroscopy was also used to further investigate the composition and microstructure of the composite. As shown in Fig. 2, the Raman spectra derived from the as-synthesized $Ni(OH)_2$ /MWCNTs and NiO /MWCNTs samples have four peaks in the range of $225\text{--}2000 \text{ cm}^{-1}$, which includes peaks associated to Raman active vibrational modes of $NiO/Ni(OH)_2$ and MWCNTs. The peaks located at the 1578 and 1348 cm^{-1} represent G and D bands of graphene. The G band is a radial C–C stretching mode of sp^2 bonded carbon, while the D band is a first-order zone boundary phonon mode

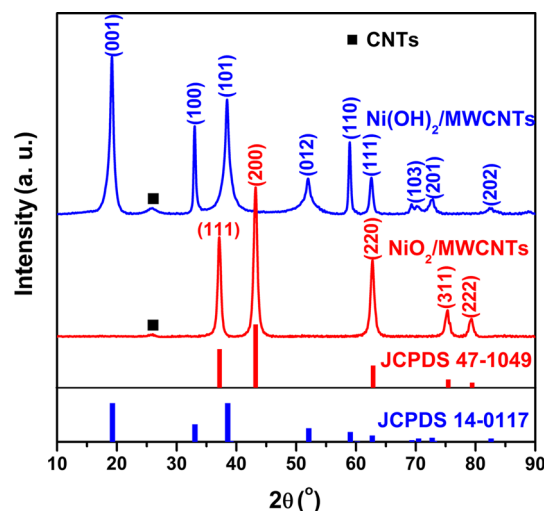


Fig. 1 XRD patterns of $Ni(OH)_2$ /MWCNTs and NiO /MWCNTs composite

associated with the defects in the graphene or graphene edge [23, 24]. The intensity ratio of D band to G band (I_D/I_G) reflects the degree of the defects in the graphene or the edges. After annealing treatment, a weak D band can be found, indicating a low density of defects and disorder of

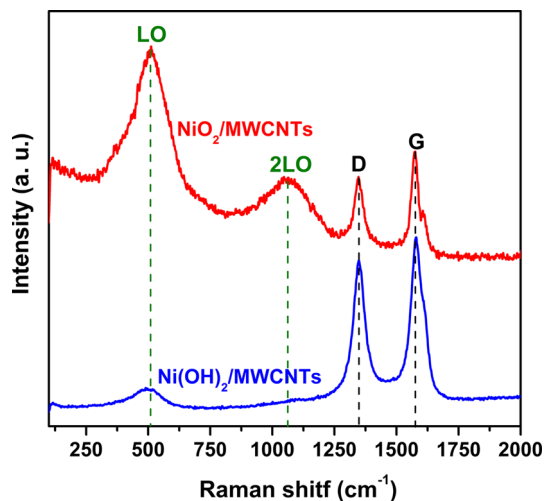


Fig. 2 Raman spectra of $\text{Ni(OH)}_2/\text{MWCNTs}$ and NiO/MWCNTs composite

the graphitized structure. Except for the typical D and G peaks attributed to graphene, two characteristic peaks at 509 and 1060 cm^{-1} , respectively, can be identified clearly and identified as longitudinal optical (LO) and 2LO phonon modes of Ni–O stretching mode [25]. The Raman spectra of $\text{Ni(OH)}_2/\text{MWCNTs}$ and NiO/MWCNTs also confirmed that the $\text{Ni(OH)}_2/\text{MWCNTs}$ successfully converted to NiO/MWCNTs by annealing treatment at 400 °C for 2 h in air.

SEM micrograph and microstructure of the resulting products are presented in Fig. 3. From the low and high magnification images, they show that the uncalcined and the calcined samples exhibit similar shaped features. The MWCNTs were well dispersed in the Ni(OH)_2 or NiO and form a network among Ni(OH)_2 or NiO powders, as shown in Fig. 3. SEM images of the composites demonstrate that the Ni(OH)_2 or NiO has an aggregated flake-like morphology with CNTs dispersed in the oxide matrix interconnecting the aggregates. It can be noted that the MWCNTs diameters are in the range of 20–40 nm, which are smaller than those of the pristine sample, and furthermore the MWCNTs are more severely curved in the nanocomposite.

Further investigation of these samples was performed by TEM and HRTEM. Figure 4 shows the typical images of

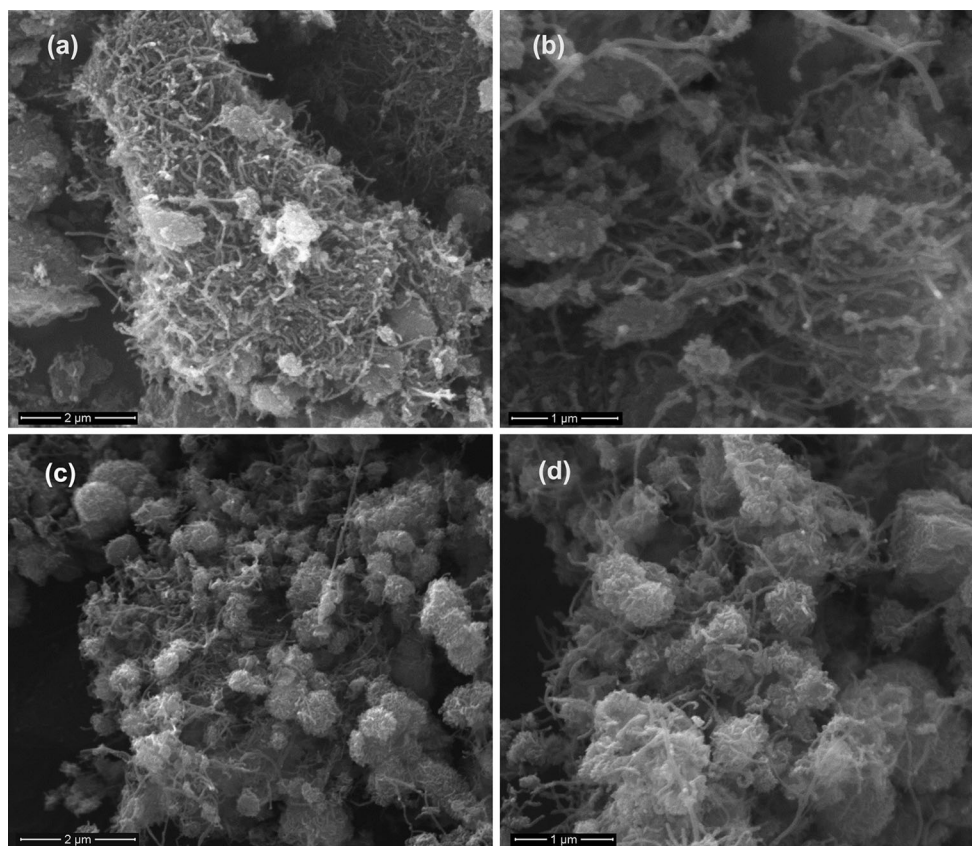


Fig. 3 SEM images of **a** and **b** $\text{Ni(OH)}_2/\text{MWCNTs}$, **c** and **d** NiO/MWCNTs composite at different magnifications, respectively

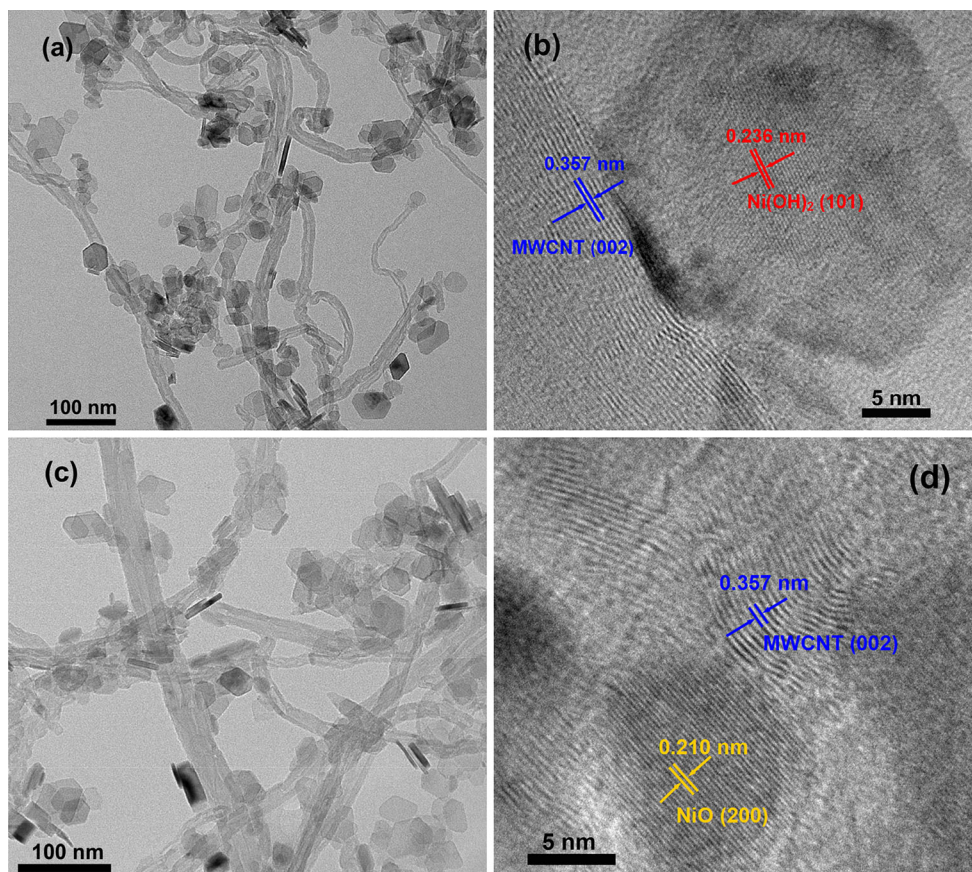


Fig. 4 TEM and HRTEM images of **a** and **b** $\text{Ni}(\text{OH})_2/\text{MWCNTs}$, **c** and **d** NiO/MWCNTs composite at different magnifications, respectively

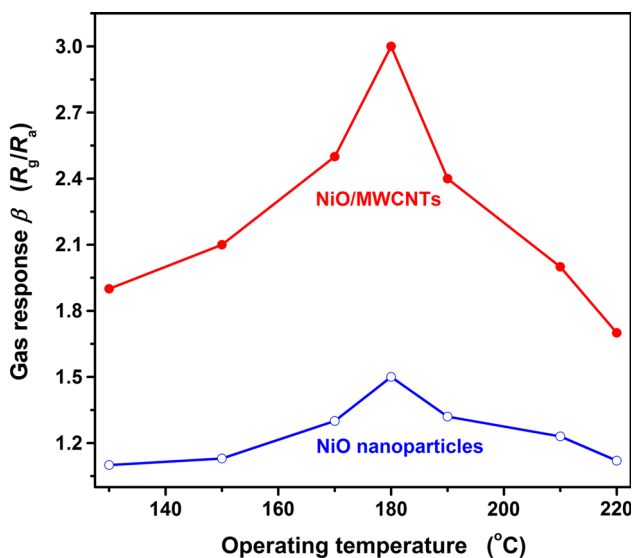


Fig. 5 Gas responses of NiO/MWCNTs composite and NiO nanoparticles based sensors to ethanol gas of 500 ppm at the different operating temperature

$\text{Ni}(\text{OH})_2/\text{MWCNTs}$ and NiO/MWCNTs nanostructures. The MWCNT diameter was observed to be 20–35 nm. $\text{Ni}(\text{OH})_2$ or NiO nanoparticles randomly disperse on the

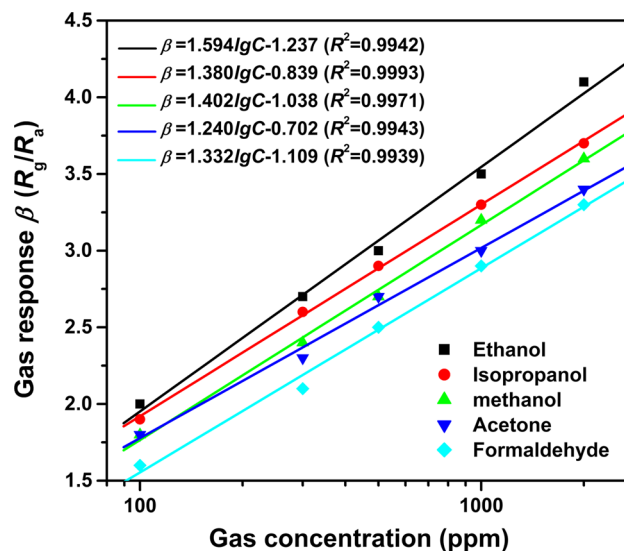


Fig. 6 Response variation of sensor to different target gases under the different gas concentrations at the operating temperature of 180 °C

MWCNTs. The HRTEM observation further reveals that $\text{Ni}(\text{OH})_2$ or NiO nanocrystals are anchored and directly grow on the MWCNTs surface. The particle size of

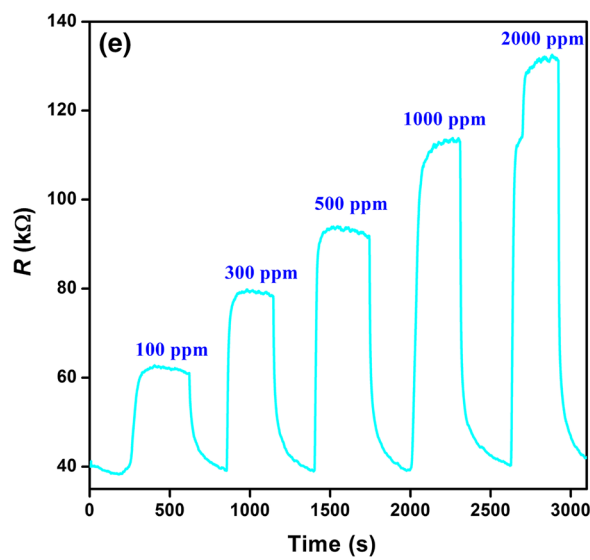
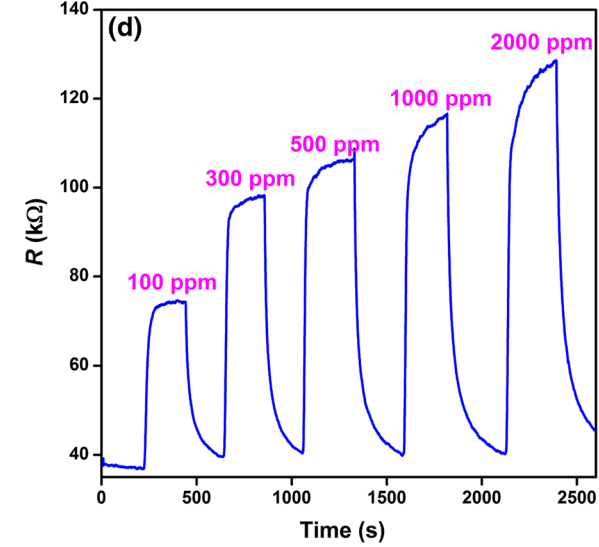
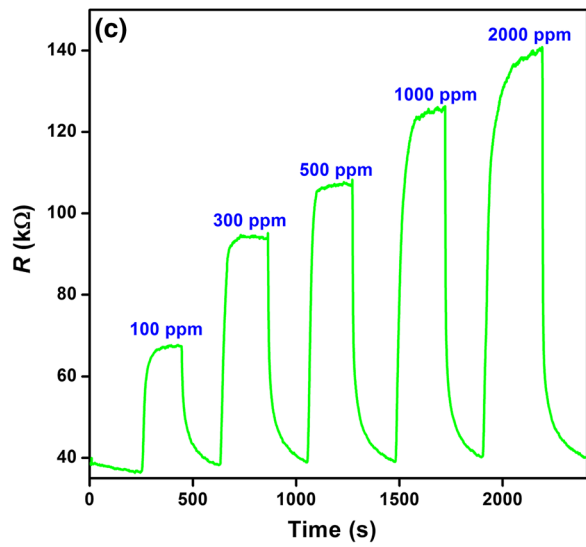
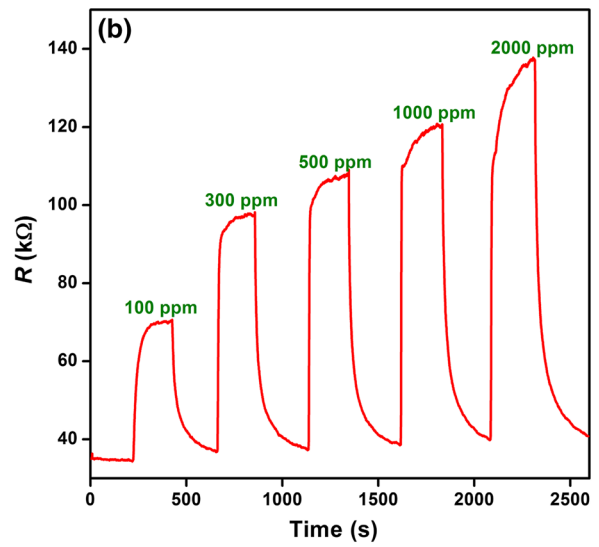
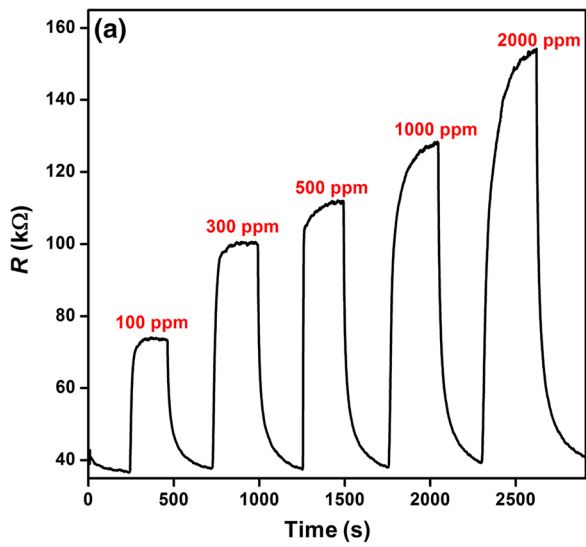


Fig. 7 Dynamic response to different gas concentration from 100 to 2000 ppm at the operating temperature of 180 °C for different target gases: **a** ethanol, **b** isopropanol, **c** methanol, **d** acetone, and **e** formaldehyde, respectively

Ni(OH)₂ is around 31 nm. The particle size of NiO decreases to 25 nm in NiO/MWCNT nanocomposite. HRTEM image of Ni(OH)₂/MWCNTs composite shown in Fig. 4b indicates that the flake-like is structurally uniform with an interplanar spacing of about 0.236 nm, which corresponds to the (101) plane of hexagonal Ni(OH)₂. While the lattice fringe with an interplanar distance of 0.357 nm can be attributed to the (002) plane of MWCNTs. As shown in Fig. 4d, the interplanar spacing of about 0.21 nm corresponds to the (200) plane of cubic NiO for NiO/MWCNTs composite, illustrating the formation of crystalline NiO nanoparticles on MWCNTs.

The MWCNTs surface was covered the functional groups (hydroxyl groups) under the preparation procedure. The hydrated positively charged Ni²⁺ ions were attracted and bound onto negatively charged CNT surfaces by electrostatic attraction and hydrogen bond with –OH. Subsequently, it promotes the nucleation of Ni(OH)₂ crystals. On the other hand, most of the hydrate of Ni²⁺ formed with solution of NH₄OH and NiCl₂ can ceaselessly assemble to the surface of MWCNTs, which provides a higher potential for the precipitation of Ni(OH)₂ nuclei on the surfaces of MWCNTs. The Ni(OH)₂ was calcined at high temperature to form the oxide. The similar formation mechanisms were reported [26] and the generating Ni(OH)₂/MWCNTs and NiO/MWCNTs in relatively large quantities can be synthesized.

To evaluate the potential applicability in gas sensor for VOCs, we investigated fundamental gas sensing properties of the as-synthesized NiO/MWCNTs composite and NiO nanoparticles, respectively. It has been addressed that the electrical conductivity of a sensor not only depends on the gas atmosphere, but also on the operating temperature of the sensing material exposed to the test gas [27]. Therefore, in order to keep the stability of a sensor, choosing an optimal operating temperature is undoubtedly necessary. Figure 5 shows the variation in the gas response with operating temperature in the presence of ethanol. The ethanol concentration was kept constant at 500 ppm. One can see that the operating temperature has a great influence on the response. When the operating temperature varies from 160 to 180 °C, the gas response first increases and then decreases, and has the maximum sensitivity at 180 °C. This behaviour was already observed in other sensor materials [28, 29]. As shown in Fig. 5, it can be seen that the NiO/MWCNTs composite based sensor shows better gas response to ethanol gas than that of NiO nanoparticles exhibited the highest response to ethanol gas at same

operating temperature. Therefore, this temperature has been chosen for monitoring different VOCs gases.

The gas responses measured at the operating temperature of 180 °C also showed a good dependence on the VOCs gas concentrations. As shown in Fig. 6, the gas responses of the NiO/MWCNTs composite based sensors show good dependence on the different VOCs gas concentrations. The straight lines of sensor are the calibration curves and the experimental data were fitted as:

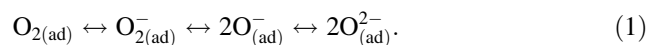
$$\beta = m \lg C_{\text{gas}} + k$$

where m is the gas response coefficient, C_{gas} is the gas concentration of the different VOCs gases, and k is a constant. The correlative coefficients R^2 are more than 0.99 indicating a good linear dependence.

Figure 7 shows the dynamic response and the gas concentration dependence of NiO/MWCNTs composite. As p-type semiconductors, the resistance of the sensors increased greatly when they exposed to the reducing gas. Then the resistance value can recover to the initial level quickly after the sensors removed from the gas atmosphere. As important parameters for tailoring sensor for practical application, the response time and recovery time (defined as the time required to reach 90 % of the final equilibrium value) of NiO/MWCNTs composite in 100 ppm ethanol, isopropanol, methanol, acetone, and formaldehyde are 27 and 87 s, 57 and 137 s, 54 and 94 s, 25 and 86 s, 142 and 84 s respectively. On the other hand, NiO/MWCNTs composite presents good repetition property. On and off cycles could be repeated several times, and any major changes in the response were observed.

Table 1 shows a brief summary of the sensing performances of various NiO nanostructures based gas sensor toward VOCs. As it has been introduced, the gas responses of pure NiO nanostructures toward VOCs are poor [2, 30–33]. By composing NiO with MWCNTs can significantly promote its gas response. And the as-synthesized NiO/MWCNTs composite in this work shows the higher gas response and lower operating temperature.

NiO is a typical p-type semiconductor in air, and its gas-sensing mechanism is based on the changes before and after exposed to the test gas. When the sensors based on NiO oxides exposed to the air by heating, the oxygen chemically adsorbed on the surface undergoes the following reactions [34]:



The oxygen captures electrons from the material, leading to the increase in concentration of holes. Hence, the conductivity of the sensors increased due to the increasing concentration of available carrier. When the sensors exposed to the reducing gas such as ethanol, acetone, or formaldehyde in our study, the interaction between the

Table 1 Comparison of varied nickel oxide nanostructures in VOCs sensing performances

Materials	β	Optimal temperature (°C)	Response time/recovery time (s)	References
NiO nanoparticles	1.30 (100 ppm acetone)	350	Non-giving	Zeng et al. [30]
	1.25 (100 ppm formaldehyde)			
	1.10 (100 ppm ethanol)			
NiO nanowires	3.30 (500 ppm ethanol)	300	480/300	Liu et al. [31]
	2.40 (500 ppm ethanol)	350	19/22	Miao et al. [32]
	1.70 (1150 ppm acetone)		21/30	
	3.35 (500 ppm ethanol)	300	4–5/6–10	Zhu et al. [33]
NiO nanoblocks	1.14 (500 ppm ethanol)	300	4–5/6–10	Zhu et al. [33]
NiO nanorods	1.42 (500 ppm ethanol)	300	4–5/6–10	Zhu et al. [33]
NiO nanoplatelets	3.10 (800 ppm ethanol)	350	Non-giving	Chu et al. [34]
NiO hollow spheres	1.55 (100 ppm acetone)	350	Non-giving	Zeng et al. [30]
	1.35 (100 ppm formaldehyde)			
	1.30 (100 ppm ethanol)			
NiO/MWNTs	1.60 (100 ppm formaldehyde)	180	142/84	This work
	1.80 (100 ppm acetone)		25/86	
	2.00 (100 ppm ethanol)		27/87	
	1.80 (100 ppm methanol)		54/94	
	1.90 (100 ppm isopropanol)		57/137	

reducing gas and the oxygen adsorbed on the sensors surface can be explained as [34]:



The electrons trapped by the adsorbed oxygen are released. So, a number of electrons annihilated with holes [35, 36]:



With the gas concentration increasing, this action enhances until saturation. Consequently, both the concentration of the holes in NiO and conductivity of the sensors decrease. Therefore the changes in conductance determine the sensitivity of the sensors.

In view of the sensing mechanism, many factors including the particle size, defects, the properties of surface and interface, the barrier height/width, and stoichiometry directly affect the state and amount of oxygen species on the surface of sensors, and consequently the performance of the metal oxide-based sensors [29]. Among these factors, the effects of particle size have been the focus of many reports. The smaller particles can offer more active sites for adsorption of gas molecules due to their large surface area, which provide more surface sites available for oxygen to be adsorbed on them and to make contact with the surrounding gases [37]. NiO nanoparticles anchored and directly grown on the MWCNTs surface will decrease the aggregation of NiO nanoparticles, which led to higher specific surface than that of individual NiO

nanoparticles. In addition to the surface area, the number of contact points between individual MWCNTs is also an important factor affecting the performance of the sensor [38]. If individual MWCNTs are interconnected, a continuous pathway for charge carriers is provided, which can transfer charge carriers into electrodes. Upon adding NiO nanoparticles to the MWCNTs, further inter-connections of individual MWCNTs are generated. On the other hand, inter-connections let electrons easily get over the barriers and decrease the operating temperature. Therefore, a large surface area and numerous contacts between the MWCNTs result in stronger interactions between NiO/MWCNTs composite and VOCs gases, exhibiting an even improved gas-sensing property.

4 Conclusion

NiO/MWCNTs composite was successfully prepared and used to detect VOCs gases. The as-prepared nanocomposites were characterized by means of X-ray diffraction, Raman spectrum, and transmission electron microscopy. It was indicated that NiO nanoparticles with size of about 25 nm were decorated on the MWCNTs. The chemoresistive gas sensor performance of the as-prepared NiO/MWCNTs composite to VOCs gases was investigated. NiO/MWCNTs composite exhibited higher response for detecting VOCs gases than that of pure NiO nanoparticles. Enhancement of sensor response may be attributed to

higher surface area and inter-connections of NiO/MWCNTs composite, which offer more active sites for adsorption of gas molecules, easily get over the barriers and decrease the operating temperature.

Acknowledgments This work was supported by the National Natural Science Foundation of China (Grant No. 51262029), the Key Project of the Department of Education of Yunnan Province (ZD2013006), and Yunnan University Graduate Program for Research and Innovation (ynuy201392).

References

- C.J. Dong, X.C. Xiao, G. Chen, H.T. Guan, Y.D. Wang, *RSC Adv.* **5**, 4880–4885 (2015)
- G.X. Zhu, C.Y. Xi, H. Xu, D. Zheng, Y.J. Liu, X. Xu, X.P. Shen, *RSC Adv.* **2**, 4236–4241 (2012)
- N.D. Hoa, S.A. El-safty, *Chem. Eur. J.* **17**, 12896–12901 (2011)
- B. Liu, H. Yang, H. Zhao, L. An, L. Zhang, R. Shi, L. Wang, L. Bao, Y. Chen, *Sens. Actuators B* **156**, 251–265 (2011)
- N.G. Cho, H.S. Woo, J.H. Lee, I.D. Kim, *Chem. Commun.* **47**, 11300–11302 (2011)
- N.G. Cho, I.S. Hwang, H.G. Kim, J.H. Lee, I.D. Kim, *Sens. Actuators B* **155**, 366–371 (2011)
- G. Mattei, P. Mazzoldi, M.L. Post, D. Buso, M. Guglielmi, A. Martucci, *Adv. Mater.* **19**, 561–564 (2007)
- H.J. Kim, K. Choi, K.M. Kim, C.W. Na, J.H. Lee, *Sens. Actuators B* **171**, 1029–1037 (2012)
- J. Wang, L.M. Wei, L.Y. Zhang, J. Zhang, H. Wei, C.H. Jiang, Y.F. Zhang, *J. Mater. Chem.* **22**, 20038–20047 (2012)
- L.L. Wang, J.N. Deng, T. Fei, T. Zhang, *Sens. Actuators B* **164**, 90–95 (2012)
- L. Xu, R.F. Zheng, S.H. Liu, J. Song, J.S. Chen, B. Dong, H.W. Song, *Inorg. Chem.* **51**, 7733–7740 (2012)
- L.L. Wang, Z. Lou, R. Wang, T. Fei, T. Zhang, *J. Mater. Chem.* **22**, 12453–12456 (2012)
- U. Kirner, K.D. Schierbaum, W. Gopel, B. Leibold, N. Nicoloso, W. Weppner, D. Fischer, W.F. Chu, *Sens. Actuators B* **1**, 103–107 (1990)
- M. Zhang, L.L. Brooks, N. Chartuprayoon, W. Bosze, Y.H. Choa, N.V. Myung, *ACS Appl. Mater. Interfaces* **6**, 319–326 (2014)
- C. Balázs, K. Sedláčková, E. Llobet, R. Ionescu, *Sens. Actuators B* **133**, 151–155 (2008)
- G.H. Lu, L.E. Ocola, J.H. Chen, *Adv. Mater.* **21**, 2487–2491 (2009)
- N.V. Hieu, L.T.B. Thuy, N.D. Chien, *Sens. Actuators B* **129**, 888–895 (2008)
- N.D. Hoa, N.V. Quy, Y.S. Cho, D. Kim, *Phys. Status Solidi (a)* **204**, 1820–1824 (2007)
- J.M. Tulliani, A. Cavalieri, S. Musso, E. Sardella, F. Geobaldo, *Sens. Actuators B* **152**, 144–154 (2011)
- D. Jung, M. Han, G.S. Lee, *Carbon* **78**, 156–163 (2014)
- M.H. Cao, Y.D. Wang, T. Chen, M. Antonietti, M. Niederberger, *Chem. Mater.* **20**, 5781–5786 (2008)
- D. Hu, B.Q. Han, S.J. Deng, Z.P. Feng, Y. Wang, J. Popovic, M. Nuskol, Y.D. Wang, I. Djerdj, *J. Phys. Chem. C* **118**, 9832–9840 (2014)
- Y. Liu, L. Liu, P. Liu, L. Sheng, S. Fan, *Diam. Relat. Mater.* **13**, 1609–1613 (2004)
- H. Murphy, P. Papakonstantinou, T.I.T. Okpalugo, *J. Vac. Sci. Technol. B* **24**, 715–720 (2006)
- X. Li, A. Dhanabalan, K. Bechtold, C. Wang, *Electrochem. Commun.* **12**, 1222–1225 (2010)
- K. Dai, C.H. Liang, J.M. Dai, L.H. Lu, G.P. Zhu, Z.L. Liu, Q.Z. Liu, Y.X. Zhang, *Mater. Chem. Phys.* **143**, 1344–1351 (2014)
- G. Eranna, B.C. Joshi, D.P. Runthala, R.P. Gupta, *Crit. Rev. Solid State Mater. Sci.* **29**, 111–188 (2004)
- T. Chen, Q.J. Liu, Z.L. Zhou, Y.D. Wang, *Nanotechnology* **19**, 095506 (2008). (5 pp)
- X.Y. Cai, D. Hu, S.J. Deng, B.Q. Han, Y. Wang, J.M. Wu, Y.D. Wang, *Sens. Actuators B* **198**, 402–410 (2014)
- W. Zeng, B. Miao, L.Y. Lin, J.Y. Xie, *Trans. Nonferr. Met. Soc. China* **22**, s100–s104 (2012)
- B. Liu, H.Q. Yang, H. Zhao, L.H. An, L.H. Zhang, R.Y. Shi, L. Wang, L. Bao, Y. Chen, *Sens. Actuators B* **156**, 251–262 (2011)
- B. Miao, W. Zeng, L.Y. Lin, S. Xu, *Phys. E* **52**, 40–45 (2013)
- G.X. Zhu, H. Xu, Y.J. Liu, C.Y. Xi, J. Yang, X.P. Shen, J. Zhu, J.L. Yang, *J. Colloid Interface Sci.* **412**, 100–106 (2013)
- X.F. Chu, X.Q. Liu, G.Y. Meng, *Sens. Actuators B* **65**, 64–67 (2000)
- X.S. Niu, W.M. Du, W.P. Du, *Sens. Actuators B* **99**, 399–404 (2004)
- X. Liu, B. Cheng, H.W. Qin, P. Song, S.X. Huang, R. Zhang, J.F. Hu, M.H. Jiang, *J. Phys. Chem. Solids* **68**, 511–515 (2007)
- Y.D. Wang, I. Djerdj, M. Antonietti, B. Smarsly, *Small* **4**, 1656–1660 (2008)
- L. Valentini, C. Cantalini, I. Armentano, J.M. Denny, L. Lozzi, S. Santucci, *J. Vac. Sci. Technol. B* **21**, 1996–2000 (2003)